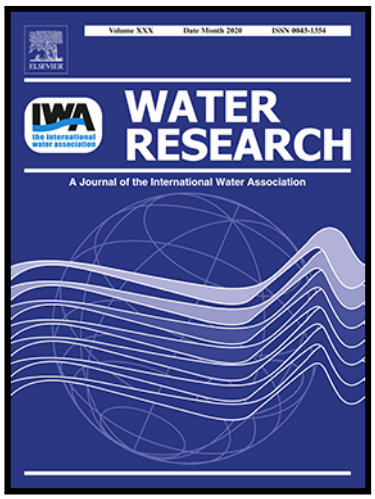

Catalyst-free activation of permanganate under visible light irradiation for sulfamethazine degradation: Experiments and theoretical calculation

Chen Zhang , Suhong Tian , Fanzhi Qin , Yali Yu , Danlian Huang , Abing Duan , Chengyun Zhou , Yang Yang , Wenjun Wang , Yin Zhou , Hanzhuo Luo

PII: S0043-1354(21)00113-5
DOI: https://doi.org/10.1016/j.watres.2021.116915
Reference: WR 116915

To appear in: *Water Research*

Received date: 10 December 2020
Revised date: 5 February 2021
Accepted date: 6 February 2021

Please cite this article as: Chen Zhang , Suhong Tian , Fanzhi Qin , Yali Yu , Danlian Huang , Abing Duan , Chengyun Zhou , Yang Yang , Wenjun Wang , Yin Zhou , Hanzhuo Luo , Catalyst-free activation of permanganate under visible light irradiation for sulfamethazine degradation: Experiments and theoretical calculation, *Water Research* (2021), doi: https://doi.org/10.1016/j.watres.2021.116915

Highlights:

- Visible light shows synergistic effect with PM for SMT degradation.
- The generation of $\bullet O_2^-$ was notably enhanced under visible light irradiation.
- Mn (III) and $\bullet O_2^-$ are responsible for SMT removal.
- Experiments and DFT are creatively combined to explore the degradation mechanism.

Catalyst-free activation of permanganate under visible light irradiation for sulfamethazine degradation： Experiments and theoretical calculation

Chen Zhang [a, b, *], Suhong Tian [a, b], Fanzhi Qin [a, b], Yali Yu [a, b], Danlian Huang [a, b, *], Abing Duan [a, b, *], Chengyun Zhou [a, b], Yang Yang [a, b], Wenjun Wang [a, b], Yin Zhou [a, b], Hanzhuo Luo [a, b]

[a] *College of Environmental Science and Engineering, Hunan University, Changsha, 410082, P.R. China*

[b] *Key Laboratory of Environmental Biology and Pollution Control, Ministry of Education, Hunan University, Changsha 410082, P.R. China*

[*] Corresponding author: College of Environmental Science and Engineering, Hunan University, Changsha, Hunan 410082, China.

E-mail: zhangchen@hnu.edu.cn (C. Zhang); huangdanlian@hnu.edu.cn (D. Huang); duanabing@hnu.edu.cn (A. Duan).

Abstract

In this study, visible light (VL) was adopted for permanganate (PM) activation without additional catalyst, where sulfamethazine (SMT) was selected as the probe compound. Experiment results showed that the VL/PM system can effectively degrade SMT through pseudo-first-order reaction kinetics. Influencing factors including PM dosage, solution pH, humid acid (HA) and coexisting anions (CO_3^{2-}, SO_4^{2-}, Cl^- and NO_3^-) which affect SMT photo-degradation were also examined. Pyrophosphate (PP) had an inhibitory effect on SMT degradation due to the complexation of PP with Mn (III). Electron spin resonance (ESR) spectrometry and UV-Vis spectrophotometer proved that VL can activate PM to generate $\bullet O_2^-$ and Mn (III) reactive species. Furthermore, based on the active site prediction, intermediates identification and Density Functional Theory (DFT) calculation, two main degradation pathways involving SMT molecular rearrangement and cleavage of S–N bond were proposed. Moreover, the energy barriers of the two degradation pathways were also calculated. This study offers a novel approach for aqueous SMT removal and deepens our understanding of the degradation mechanism of SMT through DFT calculation, which hopes to shed light on the future development of VL/PM treatment.

Keywords: Permanganate; Sulfamethazine; Trivalent manganese; Superoxide radical; Degradation pathway; Density Functional Theory

1. Introduction

As an important class of broad-spectrum antibiotics, sulfonamides are widely used in human medicine, aquaculture, and livestock production (Tian et al., 2020; Zhang et al., 2016a). However, due to their incomplete metabolism and uncontrolled release, these compounds with high levels of concentrations were detected in natural environment (Qin et al., 2020). Due to their persistence and toxicity, sulfonamides residues have led to the development and spread of sulfonamide resistance in environmental pathogens (Zhou et al., 2019b). Sulfamethazine (SMT), as a typical sulfonamide, is widespread in river, soil, sediment, underground water, and sewage plant treatment effluents (Fan et al., 2015). The reported residual concentrations generally range from ng/L to μg/L (Fan et al., 2015). The undesirable SMT residues show strongly adverse effects, such as endocrine disruption to humans and animals, chronic toxicity to human's body (Zhang et al., 2019). In addition, long-term exposure causes the emergence of resistance in intestinal microorganisms, further binding to pathogens through horizontal gene transfer. Therefore, conducting an efficient method to remove SMT in the environment is essential to protect the ecosystem and human health.

To date, various chemical oxidation techniques have been used to degrade SMT in aqueous phase (Yang et al., 2020), including oxidation by ferrate (VI) (Feng et al., 2018), chlorine or ozone (Liu et al., 2019a), advanced oxidation processes (AOPs) such as Fenton or Fenton-like (Cheng et al., 2019; Cheng et al., 2018), photocatalysis (Zhou et al., 2019a), UV/H_2O_2 and UV/persulfate (Acosta-Rangel et

al., 2018; Zhang et al., 2016b). Compared with other oxidants, permanganate (PM，$KMnO_4$) has the advantages of relatively stable, ease of storage and delivery, wide pH operating range and high standard redox potential (0.558 V ~ 1.692 V) (Yan et al., 1999). These characteristics allow PM to be successfully applied to remove various recalcitrant pollutants, such as chlorophene (Xu et al., 2018), triclosan (Gao et al., 2018) and microcystins (Kim et al., 2018). However, there is limited knowledge on the treatment of sulfonamides (e.g., SMT) with PM. This may due to the fact that PM only reacts with contaminants containing electron-rich organic moieties (PM is a selective oxidant) (Gao et al., 2014). To solve this problem, some activation methods such as some ligands (Hu et al., 2017; Jin et al., 2010) (e.g., ethylenediaminetetraacetic acid (EDTA), sodium pyrophosphate (PP), humic acid (HA)), bisulfite (Feng et al., 2018; Zhong and Zhang 2019), iodide (Li et al., 2018), are employed to activate PM to produce reactive manganese species (e.g., manganite [Mn(VI)], hypomanganate [Mn(V)] and trivalent manganese [Mn(III)]). Although the addition of these external reagents appear to be valid, they are either toxic or cause an increase in organic carbon content. Therefore, it is difficult to apply into large-scale water treatment.

Light radiation is commonly employed to activate oxidants (e.g., H_2O_2, persulfate, monochloramine) to enhance the generation of reactive radicals (Bu et al., 2018; Miklos et al., 2019) (e.g., •OH, $SO_4^{\bullet-}$, Cl•, NH_2• etc.), thus increasing the degradation of contaminants. Moreover, photolysis is also an important decay process of SMT in natural water. Previous studies observed that PM

photodecomposition will produce higher reactive manganese such as MnO_2 and MnO_2^- (Guo et al., 2018; Lee et al., 1987), as shown in (Eq. (1)) and (Eq. (2)). Thus, we have reason to believe that the use of visible light (VL) radiation can effectively activate PM and generate highly reactive species. However, there is no information on the contribution of these high-valent manganese intermediates in the presence of PM under VL system (refer as VL/PM system). Meanwhile, information on sulfonamides removal such as SMT mechanism by PM under VL system is inconclusive. Consequently, investigating the effects of light irradiation on the PM activation performance and mechanism for organic compound degradation using both experimental and theoretical calculation methods, taking SMT with light irradiation as an example, will be highly useful and promising.

$$MnO_4^- + h\nu = MnO_2^- + O_2 \quad (1)$$

$$MnO_4^- + h\nu = MnO_2 + O_2^- \quad (2)$$

In this study, we systematically investigated the degradation of SMT under the VL/PM system. The present paper focuses on the following points: (i) investigate the efficiency of VL irradiation on the PM activation; (ii) discuss the effect of solution pH, PM dosage, anions (CO_3^{2-}, SO_4^{2-}, Cl^-, and NO_3^-) and HA concentration on the degradation of SMT in the VL/PM system; (iii) evaluate the feasibility of the VL/PM process for SMT removal in natural waters; (iv) determine reactive species in the VL/PM process; (v) identify the oxidation products by high-performance liquid chromatography-triple quaternary rod tandem mass spectrometer (HPLC-MS) and propose the degradation pathways and verify by Density Functional Theory (DFT)

calculation.

2. Materials and methods

2.1. Materials

SMT was purchased from Sinopharm Chemical Reagent Co., Ltd. Its physicochemical properties were listed in Table S1. Potassium permanganate ($KMnO_4$), acetic acid (HAc), sodium hydroxide (NaOH) and p-benzoquinone (BQ) were also obtained from Sinopharm Chemical Reagent Co., Ltd. All other chemicals used in this work were at least analytical grade. Ultrapure water (> 18.2 MΩ cm) was used for the preparation of aqueous solutions.

Stock solutions of Mn (VII) (40 mM) were prepared by dissolving $KMnO_4$ crystals in ultrapure water.

2.2. Experimental procedures

All photochemical experiments is conducted in 150 mL quartz beakers under magnetic agitation (400 r/min) in the absence/presence VL (300W Xe lamp with a cut off filter (λ > 420 nm), light intensity is about 300 mW/cm^2). 300W Xe lamp is turned on 5 min to ensure a relatively stable output in the light experiment. The VL reaction system is the same as our previous research (Wang et al., 2020). Typically, 50 μM of PM is added into the solution containing 10 mg/L SMT. At pre-determined times (0, 10, 20, 30, 45, 60, 90 min), about 1 mL of the sample is filtered with 0.22 μm filter membrane, and rapidly transferred into a 2 ml chromatography sample bottle vials containing 100 μL of 1 M hydroxylamine hydrochloride to terminate the reaction. The solution pH is adjusted by 0.1 M HAc and 0.1 M of NaOH. All

experiments are performed at least in triplicate, and the mean values are adopted to ensure reproducibility.

2.3. Analytical methods

The SMT concentration is analyzed by a high-performance liquid chromatography (HPLC, Agilent 1260, USA) equipped with a UV-vis detector. The column is C-18 column (4 μm particle size, 4.6 × 250 mm) at the temperature of 30 °C. The HPLC analysis method for SMT is based on the previous study (Qin et al., 2020) (mobile phase: 65% H_2O and 35% acetonitrile (CH_3CN), flow rate: 1 mL/min, injection volume: 20 μL, and a 266 nm detection wavelength). The concentration of residual PM is determined by TU-1810 UV-Vis spectrophotometer at 525 nm and SMT mineralization is measured by a TOC-5000A model analyzer. The generated radicals ($\bullet O_2^-$ and •OH) are examined by electron spin resonance (ESR, JES-FA200), using 5, 5-dimethyl-1-pyrroline N-oxide (DMPO) as spin-trap reagent. The oxidation byproducts of SMT are identified by HPLC-MS. The detailed description of the operation condition of HPLC-MS is provided in Text S1 in the Supplementary Material.

2.4. Theoretical calculation

The calculations of all geometric structure is performed by Gaussian 16 (Frisch et al., 2016) with the Density Functional Theory (DFT) method (Grimme et al., 2011; Hariharan and Pople 1973). The geometry optimizations are conducted using the B3LYP functional, with 6-31G(d) basis set for the all atoms. The transition states are performed with the same method and basis set, and Intrinsic Reaction Coordinate

(IRC) calculation is also conducted to ensure that the transition state does connect two related minimums. After all the structures are optimized, the single-point energies are evaluated with the M06-2X functional, with 6-311+G(d,p) basis set for the all atoms (R. et al., 1980; Zhao and Truhlar 2007; Zhao and Truhlar 2008). It is worth noting that DFT-D dispersion correction (Grimme 2011) is added to the calculations to better describe the weak interactions among molecules. Solvation effects were considered in the SMT solvation calculations and PCM implicit solvation model (Barone and Cossi 1998) was adopted. In addition, the Fukui Function (f(**r**)) (Lu and Chen 2012) is introduced to analyze vulnerable sites of SMT. Details on DFT calculation can be found in Text S2 in the Supplementary Material. These data are used to predict the site of reactive species attack on SMT during the oxidation process.

3. Results and discussions

3.1. Reaction kinetics

3.1.1. Effect of visible light radiation on PM oxidation of SMT

To investigate the roles of VL on PM activation, the degradation of SMT by VL alone (direct photolysis), PM alone and VL/PM is systematically studied, as shown in Figure 1a. When subjected to VL irradiation alone, only 2.03% of SMT is removed within 90 min. There is 34.63% removal of SMT in the presence of 50 μM PM without light irradiation. However, the addition of 50 μM PM with VL irradiation significantly enhance SMT degradation efficiency. The removal efficiency (85.50%) is much higher than the sum of the efficiencies of photolysis and

PM oxidation. Furthermore, the degradation of SMT could be well simulated by pseudo-first-order kinetics (Figure 1b), which is described as (Eq. (3)). The rate constant (k_{obs}) of the VL/PM is as high as 0.0217 min^{-1}, much higher than that of VL alone (0.0003 min^{-1}) and PM oxidation (0.0047 min^{-1}), indicating the existence of synergistic effect.

$$\ln (C_t/ C_0) = -k_{obs} * t \quad (3)$$

Where C_0 and C_t represent the concentration of SMT at reaction times of t = 0 and t = t, respectively, and k_{obs} is the pseudo-first-order rate constants (min^{-1}).

The change of PM concentration over time during PM oxidation and VL/PM process is also investigated, as shown in Figure S1. The residual PM concentration in VL/PM process is almost twice as high as that in PM oxidation after 90 min reaction, suggesting that VL irradiation can considerable alleviate the consumption of PM in the VL/PM. Based on the above results, it is reasonable to speculate that reactive species are generated in the VL/PM system (Lee et al., 1987). Therefore, the enhancement mechanism needed to be investigated in great detail.

3.1.2. Effect of PM dosage

To further understand the removal efficiency of SMT in VL/PM process, the effect of different concentrations of PM on SMT degradation is studied. Figure 1c shows that SMT degradation obviously relies on PM dosage. The removal efficiency of SMT increases from 2.03% to 99.08% when PM dosage increases from 0 to 200 μM. Correspondingly, the k_{obs} increases from 0.0003 min^{-1} to 0.0555 min^{-1} (Figure 1d). The phenomenon indicates that higher PM dosage lead to a better degradation

efficiency and degradation rate, which is different from the traditional AOPs that had an optimum dosage of oxidizer (Xue et al., 2020). However, excess oxidant can lead to an unnecessary consumption of PM. Thus, unless otherwise stated, the selected PM dosage is 50 μM in the following experiments.

3.1.3. Effect of solution pH

It is widely accepted that pH condition affected the oxidation ability and stability of PM because of the existence of various acid-base dependent Mn (VII) species. And the speciation of SMT is highly dependent on environmental pH (Figure S2) (Gao et al., 2012; Zhang et al., 2016a). Thus, solution pH may play a significance role in compound reactivity. In this study, the effect of solution pH (3.93-10.85) on the VL/PM system for SMT removal is evaluated. As shown in the Figure 2a, 83.47% of SMT is removed at pH 3.93 within 45 min, while only 2.93% is removed at pH 10.85 within 90 min. In addition, Figure S3 depicts the variation of k_{obs} with the solution pH change. It can be seen that the degradation rates of SMT decreases gradually with the increasing solution pH. With the increase of solution pH from 3.93 to 10.85, k_{obs} drops sharply from 0.0305 min^{-1} to 0.0005 min^{-1}. As a result, an acidic circumstance is more conducive to SMT removal in the VL/PM system.

The reasons may be that PM has undergone a series of disproportionation and reduction reactions under acidic conditions, eventually leading to manganese oxide (MnO_2) or Mn (II) as the final product. In addition, the redox potential of Mn (VII) under acidic conditions (1.51 V, Eq. (4)) is higher than that of under neutral conditions (0.58 V, Eq. (5)) and alkaline conditions (0.56 V, Eq. (6)) (Hu et al., 2018).

Meanwhile, the in-situ generation of MnO_2 shows more reactive under acidic conditions, which is favorable for SMT degradation (Xu et al., 2018). Previous studies also demonstrated that MnO_2 could accelerate the oxidation kinetics of organics in the process of PM oxidation (Gao et al., 2012; Hu et al., 2018). Therefore, acidic condition is conducive to improving the oxidation ability of PM.

$$MnO_4^- + 8\ H^+ + 5\ e^- = Mn^{2+} + 4\ H_2O \quad (4)$$

$$MnO_4^- + 2\ H_2O + 3\ e^- = MnO_2 + 4\ OH^- \quad (5)$$

$$MnO_4^- + e^- = MnO_4^{2-} \quad (6)$$

3.1.3. Effect of anions and humic acid on SMT degradation

The effect of anions (e.g., CO_3^{2-}, SO_4^{2-}, Cl^- and NO_3^-) and HA on SMT removal is evaluated by using initial PM concentration of 50 μM under VL irradiation. As shown in Figure 2b, the addition of individual SO_4^{2-}, Cl^- and NO_3^- could slightly promote the degradation of SMT. The reason is that SO_4^{2-}, Cl^- and NO_3^- play a role in delaying the decomposition of PM (Han et al., 2013), further facilitating the oxidation reaction of PM. Compared with SO_4^{2-}, Cl^- and NO_3^-, the degradation efficiency of SMT is significantly inhibited by the presence of CO_3^{2-}. To be specific, the removal efficiency is only 12.2% after 90 min in the presence of 0.5 mM. It is also observed that the value of solution pH is increased from 6.43 to 8.15. As mentioned in section 3.1.3, the redox potential of Mn (VII) is as low as 0.56 V under alkaline conditions. Liu et al., (2016) observed a similar inhibitory effect, as the addition of CO_3^{2-} would lead to the equilibration of CO_3^{2-}-HCO_3^-. Moreover, $CO_3^{\bullet-}$ is a common free radicals' scavenger (Qian et al., 2016), thus resulting in a low

efficiency.

Figure 2c shows that HA exhibited a double-edge role in the degradation of SMT in the VL/PM system. HA with a low concentration level (< 5 mg/L) has a mild effect in promoting oxidation of SMT by PM, which is ascribed to the reductive properties of HA, increasing the generation of MnO_2 (Sun et al., 2013; Yang et al., 2018). Meanwhile, HA could complex with Mn (III) (Eq. (7)) and then successively produce $O_2^{\bullet-}$ (Eq. (8)) and •OH (Eq. (9)) (Jin et al., 2010; Xu et al., 2017). However, when the HA concentration is further increased from 5 mg/L to 10 mg/L, the removal efficiency decreases from 86.34% to 65.95%. On the one hand, more PM is consumed under high level concentration of HA, which lead to the reduction of SMT removal rate. On the other hand, excessive HA could compete with target compound for secondary oxidants (e.g., MnO_2, $O_2^{\bullet-}$, •OH) (Chow and Sze-Yin Leung 2019), which also inhibits the oxidation of SMT.

$$Mn(VII) + 4\,[HA\text{-}Mn(II)] + HA \rightarrow 5\,[HA\text{-}Mn(III)] \quad (7)$$

$$2\,[HA\text{-}Mn(III)] + O_2 + 2\,H_2O \rightarrow 2\,Mn(II) + 2\,O_2^{\bullet-} + 4\,H^+ + 2\,HA \quad (8)$$

$$O_2^{\bullet-} + H_2O \rightarrow HO_2^{\bullet} + OH^- \quad (9)$$

$$HO_2^{\bullet} + H_2O \rightarrow \bullet OH + H_2O_2 \quad (10)$$

3.1.4. Degradation of SMT in different water matrices

To better understand the oxidation of SMT in natural water, four types of water such as ultrapure water (UW), tap water (TW), Xiangjiang river water (XRW) and Peach lake water (PLW) are used in the experiments. The characteristics of the four types of water are listed in Table S2. As shown in Figure 3a, the degradation of SMT

is inhibited in the three real water bodies, compared to that in UW. The tendency of TOC removal rate is consistent with SMT. When the removal efficiency of SMT is high, the TOC removal ratio is also relatively high (Figure 3b). The results indicate that coexisting substances in natural water matrices may compete with SMT for oxidants, which affects the degradation efficiency of SMT.

3.2. Identification of the reactive species

3.2.1. Reactive oxygen radicals

Firstly, the generation of reactive oxygen radicals was the most common reason why light irradiation can improve the activity of oxidants (Luo et al., 2019). According to the previous study (Guo et al., 2018), •OH and $•O_2^-$ were most likely to be produced in the oxidation process. To investigate the roles of reactive oxygen radicals played in VL/PM system, methanol (MeOH) and tert-butanol (TBA) are used as scavengers of •OH, and *p*-benzoquinone (PBQ) serves as $•O_2^-$ quencher. In the VL/PM/MeOH and VL/PM/TBA, the degradation of SMT is not inhibited but improved. There are 2.17% and 11.15% higher than that of control group (85.50%) (Figure 4a). The reason is that MeOH and TBA are transformed into alkyl radicals (R·), further increasing the reduction of PM (Hu et al., 2018). However, the addition of PBQ sharply hinders the degradation of SMT, its removal efficiency after 90 min reaction decreases from 85.50% to 34.19% as 2 mM of PBQ is added (Figure 4a). Therefore, the results indicate that $•O_2^-$ plays a dominant role, while •OH plays an insignificant role for the degradation of SMT in VL/PM system.

To further confirm the existence of radicals, ESR analysis with DMPO are

performed in MeOH and ultrapure water for $•O_2^-$ and •OH detection, respectively (Wang et al., 2020; Yin et al., 2018). It could be seen from the ESR spectrum (Figure 4b) that no signals of DMPO-$•O_2^-$ and DMPO-•OH are detected in the dark. However, the characteristic signals of DMPO-$•O_2^-$ (with an intensity ratio of 1:1:1:1) and DMPO-•OH (with an intensity ratio of 1:2:2:1) could be observed under VL irradiation, suggesting the generation of $•O_2^-$ and •OH during the VL/PM system. In particular, the peak intensity of $•O_2^-$ significantly increases with the irradiation time (from 5 min to 10 min), and its intensity signals is much higher than that of DMPO-•OH. The results confirm that $•O_2^-$ is the primary reactive oxygen radicals in the VL/PM process, which is consistent with the results of free radical trapping tests.

3.2.2. Reactive manganese species

Secondly, the generation of intermediate manganese is speculated during the activation of potassium permanganate under VL. Theoretically, intermediate manganeses involve Mn (VI), Mn (IV), Mn (III) and Mn (II), while Mn (IV) and Mn (II) are relatively stable and difficult to react with pollutants (Simandi et al., 1984). Experimental results (Figure 2a) prove that Mn (VI) does not react with SMT. To explore the activation mechanism, TU-1810 UV-Vis spectrophotometer is used to investigate the absorbance spectra of the solution at different reaction times during dark and VL system. As seen in Figure 5a-b, there is also no change in the absorption peak of Mn (VI) at 610 nm. Thus, Mn (VI) is ruled out. It is noting that the intensities of the absorption peak at 300 nm-500 nm of the reaction solution in VL/PM system are higher than that of the dark system. This is mainly due to the

accumulation of MnO_2 and Mn^{2+} (Jiang et al., 2015; Simandi et al., 1984). The result indicates that the involvement of VL promotes MnO_2 formed during the VL/PM system.

$$Mn^{3+} + e^- = Mn^{2+} \quad (11)$$

$$2\ Mn^{3+} + 2\ H_2O = MnO_2 + Mn^{2+} + 4\ H^+ \quad (12)$$

Furthermore, it is reported that Mn (III) processes a high oxidation property for one electron transfer reactions (1.54 V, Eq. (11)) (Kostka et al., 1995). With the negative free energy of reaction (ΔG), Mn (III) is labile and easily disproportionate to Mn (II) or Mn (IV) (Davies 1968) (Eq. (12)). PP is a commonly used Mn (III) complexing agent, which would lead to Mn (III)-PP formed. The formed Mn (III)-PP has a characteristic absorbance peak at 258 nm (Webb et al., 2005). To ascertain whether Mn (III) is important in the VL/PM system, the effect of PP on SMT degradation is investigated and corresponding UV-vis spectra at 200 nm-800 nm after 90 min reaction is compared. As shown in Figure 5c, the degradation of SMT is significantly suppressed by the addition of PP and the inhibiting effect increases with the increase of PP concentration (50 μM, 200 μM and 1000 μM). Adding 1000 μM of PP almost completely inhibits the degradation of SMT ($[PM]_0 = 50\ \mu M$, $[SMT]_0 = 10$ mg/L), indicating that Mn (III) plays an important role in the degradation of SMT in VL/PM system. Compared with SMT, Mn (III) is more susceptible to PP and the formed Mn (III)-PP cannot bond to SMT, thus negatively influencing its oxidation capacity (Hu et al., 2017). The characteristic peak of Mn (III) at 258 nm is also observed in UV-vis spectra (Figure 5d), with the content of

1000 μM PP. Consequently, the characteristic peak of others intermediate manganeses Mn (II) or Mn (IV) at 300 nm-500 nm is significantly decreased because the disproportionation of Mn (III) is inhibited. In contrast, there is still a characteristic peak at 300 nm-500 nm in the presence of 50 μM PP or 200 μM PP. The above results suggest that Mn (III) is decisive manganese intermediate, which not only has oxidation but also affects the formation of MnO_2 and Mn^{2+} (Figure 6a).

3.3. Reaction mechanism

3.3.1. Identification of degradation products and possible pathways

To better elucidate the oxidation pathways of SMT, the transformation products (TPs) by the VL/PM process are identified by using HPLC-MS/MS. The full chromatograms of the oxidation reaction samples at 0 min, 10 min, 30 min, 60 min and 90 min are obtained, which are presented in Figure S4a. Compared with the sample at 0 min, the intensity of SMT peak decreases with the time prolonging, which indicates new byproducts are generated. According to the chromatogram and mass spectrum, five TPs with precursor ions are identified by HPLC-MS analysis, which include 1-(4-amino-phenyl)-2-imino-4,6-dimethyl-1,2-dihydro-pyrimidine (m/z 215), 4-aminobenzenesulfonic acid (m/z 174), 4,6-dimethyl-2-pyrimidinamine (m/z 124), 4-aminophenol (m/z 110) and hydroxylated 4,6-dimethyl-2-amine-5-hydropyrimidine (m/z 140). Based on determined intermediates and previous research findings (Chen et al., 2020; Li et al., 2019; Yin et al., 2018), two possible degradation pathways of SMT by VL/PM oxidation are illustrated in Figure 6b. One of them is smiles-type rearrangement and SO_2 extrusion, resulting in the formation

of TP1 (m/z 215) (Pathway A). Neutral radical (SMT-H$^{\cdot 0}$) species act as reactants during the process. This is because SMT has a high potential for H-abstraction reactions in the presence of PM. After forming SMT-H$^{\cdot 0}$, smiles-type rearrangement will occur. Then a single electron is transferred from SMT to Mn (III) or Mn (IV) (Stone and Morgan 1984), finally forming 1-(4-amino-phenyl)-2-imino-4,6-dimethyl -1,2-dihydro-pyrimidine (m/z 215), as depicted in Figure 6c. Allart-Simon et al., (2016) also reported that free radicals attack sulfonamides to cause molecular rearrangement. Thus, once SMT$^{0\cdot}$ is formed, smiles-type rearrangement and SO_2 extrusion will occur because of intramolecular radical attack (Fan et al., 2015; Gao et al., 2012; Yang et al., 2018). The other is cleavage of S–N bond, producing TP2 (m/z 174) and TP3 (m/z 124) (Pathway B). Subsequently, TP2 will further take off a sulfur dioxide and become TP4 (m/z 110), and the hydroxylation of TP3 results in the generation of TP5 (m/z 140). For the process, one conjecture is that TP2 and TP3 are easier to attack by reactive species (e.g., Mn (VII), Mn (III), $\bullet O_2^-$), promoting the hydrolysis of SMT. Therefore, the concentration of SMT continues to decline.

3.3.2. Degradation pathways assisted by DFT Calculations

In order to further verify the above degradation pathways, the SMT molecular charge distribution and Fukui index based on DFT are performed and presented in Figure 7. The chemical structure of SMT is shown in Figure 7a. Generally, a specific atom with high condensed dual descriptors (CDD) value possesses a higher reactivity of the molecular sites, which is more susceptible to attack (Liu et al., 2019b; Yang and Parr 1985). In this study, electrophilic attack (f^-) is primary attack

mode due to the presence of electrophilic species (Mn (VII), Mn (III) and $•O_2^-$). As shown in Figure 7b-c, the N26 atom displays a lower CDD value (-0.0452) and is closely surrounded by the negative isosurface of Fukui Index, which indicates it is a priority site. Besides, for H atom of SMT, H33 (-0.0091), H32 (-0.0084), H27 (-0.0076) atom possess the lowest CDD value (see Table S3 in the Supplementary Material). Thus, they are more prone to H-abstraction reactions to produce SMT-$H^{·0}$, in which H33 and H32 are easier to take place H-abstraction reactions than that of H27. The above calculation results indicate that the proposed degradation pathways of SMT by VL/PM are reasonable.

Furthermore, the potential energy profile of the two degradation pathways is also calculated and presented in Figure 8. As seen in Figure 8a, the H33 and 27H in SMT are easily captured by •OH to produce A2 and A3, their relative potential energy is -23.4 kcal/mol and -16.8 kcal/mol, respectively. The result proves that A2 is easily converted to A3. Subsequently, A4 occurs smiles-type rearrangement reaction and finally forms A5 (-34.1 kcal/mol). For cleavage of S–N bond of SMT, there exists two different reaction paths, as depicted by Figure 8b-c. The first possibility is that $•O_2^-$ directly attacks the N atom of N-S bond to break this bond in the SMT molecule, but its energy barriers (34.1 kcal/mol) is higher than 30 kcal/mol. However, only 18.0 kcal/mol energy barriers are required to form B6 and B4 when breaking the N-S bond of SMT in the form of $•O_2H$ (protonated $•O_2^-$). This means that the latter is thermodynamically more favorable than the former. Thus, the S–N bond of SMT attacked by $•O_2H$ is discussed in the following part more thoroughly.

As seen in Figure 8c, B4 goes through hydroxylation to form B5 (4-aminobenzenesulfonic acid) (-45.5 kcal/mol), B6 occurs H-abstraction reaction to form B7 (-10.0 kcal/mol). Then, B7 transfers into B8 in the presence of Mn (III) (-52.6 kcal/mol). Finally, B8 goes through protonation to form B9 (-249.4 kcal/mol). In addition, PM can also oxidize 4-aminobenzenesulfonic acid (m/z 174) and 4,6-dimethyl-2-pyrimidinamine (m/z 124) to make the reaction proceed forward.

4. Conclusion

In summary, the combination of PM and VL is proved to be a powerful technology for degradation of SMT. Compare to VL alone and PM alone, the removal efficiency of SMT by VL/PM is largely improved because VL could accelerate the generation of reactive species (Mn (III) and $\bullet O_2^-$). The result of UV-vis spectra and ESR detection experiments prove that Mn (III) can promote the generation of $\bullet O_2^-$. The degradation of SMT by VL/PM is favored at a higher PM dosage and under acidic conditions. Among CO_3^{2-}, SO_4^{2-}, Cl^-, NO_3^- and HA, CO_3^{2-} and HA with a high concentration show obvious inhibition on the efficiency of VL/PM, which is ascribed to solution pH variation and competitive consumption of reactive species, respectively. Based on the detected intermediates and theoretical calculations, smiles-type rearrangement and SO_2 extrusion and cleavage of S–N bond are the main degradation pathways in the VL/PM system. By comparing energy barriers, we find that the breaking of S–N bond in SMT is the result of being attacked by $\bullet O_2H$. In addition, energy barrier calculations show that SMT molecular rearrangement and SO_2 extrusion is easier to occur than cleavage of S–N bond in

water phase.

Acknowledgements

This study was financially supported by the Program of the National Natural Science Foundation of China (51809090, 51879101, 21906049), the National Program for Support of Top–Notch Young Professionals of China (2014), the Program for Changjiang Scholars and Innovative Research Team in University (IRT-13R17), Hunan Provincial Science and Technology Plan Project (2018SK20410, 2017SK2243, 2016RS3026), the Natural Science Foundation of Hunan Province, China (Grant Nos. 2019JJ50077, 2019JJ50046), the Changsha Science and Technology Focus on Developing General Project (kq2004024) and the Fundamental Research Funds for the Central Universities (531118010114).

Declaration of Interest Statement
There is no conflict of interest among authors.

Figure captions:

Figure 1. Degradation of SMT by VL alone, PM oxidation, VL/PM process. (a) Degradation efficiency and (b) the corresponding degradation rate constants. (c) Effect of PM dosage on SMT degradation by VL/PM process and (d) the corresponding degradation rate constants. Reaction conditions: $[PM]_0$ = 50 μM, $[SMT]_0$ = 10 mg/L, original pH= 6.43, and T = 25 °C.

Figure 2. Effect of (a) solution pH, (b) anions ($[CO_3^{2-}]$ = $[SO_4^{2-}]$ = $[Cl^{-1}]$ = $[NO_3^-]$ = 0.5 mM) and (c) HA on VL/PM mediated degradation of SMT. Reaction conditions: $[PM]_0$ = 50 μM, $[SMT]_0$ = 10 mg/L, [HA] = 0-10 mg/L, original pH= 6.43, and T = 25 °C.

Figure 3. Oxidation performance of (a) PM and (b) TOC removal rate in different real water. Reaction conditions: $[PM]_0$ = 50 μM, $[SMT]_0$ = 10 mg/L, pH= 7.88, and T = 25 °C.

Figure 4. (a) Quenching results of different free radical scavengers. Reaction conditions: reaction time = 90 min, $[PM]_0$ = 50 μM, $[SMT]_0$ = 10 mg/L, [MeOH] = [TBA] = 40 mM, [PBQ] = 2 mM, original pH= 6.43, and T = 25 °C. (b) ESR spectra of DMPO-•O_2^- and DMPO-•OH in VL/PM system.

Figure 5. The evolution of UV-vis spectra at 200 nm-800 nm containing PM+ SMT (a) in the PM oxidation system and (b) VL/PM system. (c) The effect of PP on the degradation of SMT in VL/PM system and (d) corresponding UV-vis spectra after 90 min reaction. Reaction conditions: $[PM]_0$= 50 μM, $[SMT)]_0$=10 mg/L, pH= 6.43.

Figure 6. (a) Proposed mechanism for the reactive species under the VL/PM system.

(b) Possible degradation pathway of SMT by VL/PM; (c) Schematic diagram of pathway A: smiles-type rearrangement and SO_2 extrusion.

Figure 7. (a) SMT chemical structure (gray, carbon; white, hydrogen; red, oxygen; blue, nitrogen; yellow, sulfur), (b) Condensed Fukui index distribution on SMT, (c) the isosurface of Fukui index (The blue and green colors represent the negative and positive phases of the molecular orbital).

Figure 8. The computed potential energy profile for SMT degradation pathways (a) smiles-type rearrangement and SO_2 extrusion, (b) cleavage of S–N bond of SMT by reaction with $\bullet O_2^-$ and (c) cleavage of S–N bond of SMT by reaction with $\bullet O_2H$.

Reference

Acosta-Rangel, A., Sanchez-Polo, M., Polo, A.M.S., Rivera-Utrilla, J. and Berber-Mendoza, M.S. (2018) Sulfonamides degradation assisted by UV, UV/H_2O_2 and UV/$K_2S_2O_8$: Efficiency, mechanism and byproducts cytotoxicity. J. Environ. Manage. 225, 224-231.

Allart-Simon, I., Gerard, S. and Sapi, J. (2016) Radical Smiles Rearrangement: An Update. Molecules 21(7).

Barone, V. and Cossi, M. (1998) Quantum Calculation of Molecular Energies and Energy Gradients in Solution by a Conductor Solvent Model. Journal of Physical Chemistry A 102(11), 1995-2001.

Bu, L., Zhou, S., Zhu, S., Wu, Y., Duan, X., Shi, Z. and Dionysiou, D.D. (2018) Insight into carbamazepine degradation by UV/monochloramine: Reaction mechanism, oxidation products, and DBPs formation. Water Res. 146, 288-297.

Chen, C., Liu, L., Li, Y.X., Li, W., Zhou, L.X., Lan, Y.Q. and Li, Y. (2020) Insight into heterogeneous catalytic degradation of sulfamethazine by peroxymonosulfate activated with $CuCo_2O_4$ derived from bimetallic oxalate. Chem. Eng. J. 384.

Cheng, M., Liu, Y., Huang, D.L., Lai, C., Zeng, G.M., Huang, J.H., Liu, Z.F., Zhang, C., Zhou, C.Y., Qin, L., Xiong, W.P., Yi, H. and Yang, Y. (2019) Prussian blue analogue derived magnetic Cu-Fe oxide as a recyclable photo-Fenton catalyst for the efficient removal of sulfamethazine at near neutral pH values. Chem. Eng. J. 362, 865-876.

Cheng, M., Zeng, G., Huang, D., Lai, C., Liu, Y., Zhang, C., Wan, J., Hu, L., Zhou, C. and Xiong, W. (2018) Efficient degradation of sulfamethazine in simulated and real wastewater at slightly basic pH values using Co-SAM-SCS /H_2O_2 Fenton-like system. Water Res. 138, 7-18.

Chow, C.H. and Sze-Yin Leung, K. (2019) Transformations of organic micropollutants undergoing permanganate/bisulfite treatment: Kinetics, pathways and toxicity. Chemosphere 237, 124524.

Davies, G. (1968) Some aspects of the chemistry of manganese (III) in aqueous solution. Coord. Chem. Rev. 4(2), 199-224.

Fan, Y., Ji, Y., Kong, D., Lu, J. and Zhou, Q. (2015) Kinetic and mechanistic investigations of the degradation of sulfamethazine in heat-activated persulfate oxidation process. J. Hazard. Mater. 300, 39-47.

Feng, M., Jinadatha, C., McDonald, T.J. and Sharma, V.K. (2018) Accelerated Oxidation of Organic Contaminants by Ferrate(VI): The Overlooked Role of Reducing Additives. Environ. Sci. Technol. 52(19), 11319-11327.

Frisch, M.J., Trucks, G.W., Schlegel, H.B., Scuseria, G.E., Robb, M.A., Cheeseman, J.R., Scalmani, G., Barone, V., Petersson, G.A., Nakatsuji, H., Li, X., Caricato, M., Marenich, A.V., Bloino, J., Janesko, B.G., Gomperts, R., Mennucci, B., Hratchian, H.P., Ortiz, J.V., Izmaylov, A.F., Sonnenberg, J.L., Williams, Ding, F., Lipparini, F., Egidi, F., Goings, J., Peng, B., Petrone, A., Henderson, T., Ranasinghe, D., Zakrzewski, V.G., Gao, J., Rega, N., Zheng, G., Liang, W., Hada, M., Ehara, M., Toyota, K., Fukuda, R., Hasegawa, J., Ishida, M.,

Nakajima, T., Honda, Y., Kitao, O., Nakai, H., Vreven, T., Throssell, K., Montgomery Jr., J.A., Peralta, J.E., Ogliaro, F., Bearpark, M.J., Heyd, J.J., Brothers, E.N., Kudin, K.N., Staroverov, V.N., Keith, T.A., Kobayashi, R., Normand, J., Raghavachari, K., Rendell, A.P., Burant, J.C., Iyengar, S.S., Tomasi, J., Cossi, M., Millam, J.M., Klene, M., Adamo, C., Cammi, R., Ochterski, J.W., Martin, R.L., Morokuma, K., Farkas, O., Foresman, J.B. and Fox, D.J. (2016) Gaussian 16 Rev. C.01, Gaussian Inc. Wallingford CT.

Gao, J., Hedman, C., Liu, C., Guo, T. and Pedersen, J.A. (2012) Transformation of sulfamethazine by manganese oxide in aqueous solution. Environ. Sci. Technol. 46(5), 2642-2651.

Gao, S., Zhao, Z., Xu, Y., Tian, J., Qi, H., Lin, W. and Cui, F. (2014) Oxidation of sulfamethoxazole (SMX) by chlorine, ozone and permanganate--a comparative study. J. Hazard. Mater. 274, 258-269.

Gao, Y., Jiang, J., Zhou, Y., Pang, S.Y., Jiang, C., Guo, Q. and Duan, J.B. (2018) Does Soluble Mn(III) Oxidant Formed in Situ Account for Enhanced Transformation of Triclosan by Mn(VII) in the Presence of Ligands? Environ. Sci. Technol. 52(8), 4785-4793.

Grimme, S. (2011) Density functional theory with London dispersion corrections. Wiley Interdisciplinary Reviews-Computational Molecular Science 1(2), 211-228.

Grimme, S., Ehrlich, S. and Goerigk, L. (2011) Effect of the damping function in dispersion corrected density functional theory. J Comput Chem 32(7),

1456-1465.

Guo, K., Zhang, J., Li, A., Xie, R., Liang, Z., Wang, A., Ling, L., Li, X., Li, C. and Fang, J. (2018) Ultraviolet Irradiation of Permanganate Enhanced the Oxidation of Micropollutants by Producing HO• and Reactive Manganese Species. Environ Sci Tech Let 5(12), 750-756.

Han, Q., Dong, W.Y., Wang, H.J., Liu, T.Z., Sun, F.Y., Ying, Y.L. and Yan, X.L. (2013) Effects of coexisting anions on decolorization of azo dye X-3B by ferrate(VI) and a comparative study between ferrate(VI) and potassium permanganate. Sep. Purif. Technol. 108, 74-82.

Hariharan, P.C.P. and Pople, J.A.J.T.c.a. (1973) The influence of polarization functions on molecular orbital hydrogenation energies. 28, 213-222.

Hu, E., Zhang, Y., Wu, S., Wu, J., Liang, L. and He, F. (2017) Role of dissolved Mn(III) in transformation of organic contaminants: Non-oxidative versus oxidative mechanisms. Water Res. 111, 234-243.

Hu, Y.B., Lo, S.L., Li, Y.F., Lee, Y.C., Chen, M.J. and Lin, J.C. (2018) Autocatalytic degradation of perfluorooctanoic acid in a permanganate-ultrasonic system. Water Res. 140, 148-157.

Jiang, J., Gao, Y., Pang, S.Y., Lu, X.T., Zhou, Y., Ma, J. and Wang, Q. (2015) Understanding the role of manganese dioxide in the oxidation of phenolic compounds by aqueous permanganate. Environ. Sci. Technol. 49(1), 520-528.

Jin, J., Su-Yan, P. and Jun, M. (2010) Role of ligands in permanganate oxidation of organics. Environ. Sci. Technol. 44(11), 4270-4275.

Kim, M.S., Lee, H.J., Lee, K.M., Seo, J. and Lee, C. (2018) Oxidation of Microcystins by Permanganate: pH and Temperature-Dependent Kinetics, Effect of DOM Characteristics, and Oxidation Mechanism Revisited. Environ. Sci. Technol. 52(12), 7054-7063.

Kostka, J.E., Luther, G.W. and Nealson, K.H. (1995) Chemical and biological reduction of Mn (III)-pyrophosphate complexes potential importance of dissolved Mn (III) as an environmental oxidant. Geochim Cosmochim Acta 59(5), 885-894.

Lee, D.G., Moylan, C.R., Hayashi, T. and Brauman, J.I. (1987) Photochemistry of aqueous permanganate ion. J Am Chem Soc 109(10), 3003-3010.

Li, G.P., Zhang, K., Li, C.B., Gao, R.C., Cheng, Y.L., Hou, L. and Wang, Y.Y. (2019) Solvent-free method to encapsulate polyoxometalate into metal-organic frameworks as efficient and recyclable photocatalyst for harmful sulfamethazine degrading in water. Appl. Catal., B-Environ. 245, 753-759.

Li, J., Jiang, J., Pang, S.Y., Zhou, Y., Gao, Y., Yang, Y., Sun, S., Liu, G., Ma, J., Jiang, C. and Wang, L. (2018) Transformation of Methylparaben by aqueous permanganate in the presence of iodide: Kinetics, modeling, and formation of iodinated aromatic products. Water Res. 135, 75-84.

Liu, S., Salhi, E., Huang, W., Diao, K. and von Gunten, U. (2019a) Kinetic and mechanistic aspects of selenite oxidation by chlorine, bromine, monochloramine, ozone, permanganate, and hydrogen peroxide. Water Res. 164, 114876.

Liu, W., Li, Y., Liu, F., Jiang, W., Zhang, D. and Liang, J. (2019b) Visible-light-driven photocatalytic degradation of diclofenac by carbon quantum dots modified porous g-C3N4: Mechanisms, degradation pathway and DFT calculation. Water Res. 151, 8-19.

Liu, Y., He, X., Duan, X., Fu, Y., Fatta-Kassinos, D. and Dionysiou, D.D. (2016) Significant role of UV and carbonate radical on the degradation of oxytetracycline in UV-AOPs: Kinetics and mechanism. Water Res. 95, 195-204.

Lu, T. and Chen, F. (2012) Multiwfn: a multifunctional wavefunction analyzer. J Comput Chem 33(5), 580-592.

Luo, J., Liu, T., Zhang, D., Yin, K., Wang, D., Zhang, W., Liu, C., Yang, C., Wei, Y., Wang, L., Luo, S. and Crittenden, J.C. (2019) The individual and Co-exposure degradation of benzophenone derivatives by UV/H_2O_2 and UV/PDS in different water matrices. Water Res. 159, 102-110.

Miklos, D.B., Wang, W.L., Linden, K.G., Drewes, E. and Hubner, U. (2019) Comparison of UV-AOPs (UV/H_2O_2, UV/PDS and UV/Chlorine) for TOrC removal from municipal wastewater effluent and optical surrogate model evaluation. Chem. Eng. J. 362, 537-547.

Qian, Y., Guo, X., Zhang, Y., Peng, Y., Sun, P., Huang, C.H., Niu, J., Zhou, X. and Crittenden, J.C. (2016) Perfluorooctanoic Acid Degradation Using UV-Persulfate Process: Modeling of the Degradation and Chlorate Formation. Environ. Sci. Technol. 50(2), 772-781.

Qin, F., Peng, Y., Song, G., Fang, Q., Wang, R., Zhang, C., Zeng, G., Huang, D., Lai,

C., Zhou, Y., Tan, X., Cheng, M. and Liu, S. (2020) Degradation of sulfamethazine by biochar-supported bimetallic oxide/persulfate system in natural water: Performance and reaction mechanism. J. Hazard. Mater. 398.

R., Krishnan, J., S., Binkley, R., Seeger, J., A. and Physics, P.J.J.o.C. (1980) Self‐consistent molecular orbital methods. XX. A basis set for correlated wave functions.

Simandi, L.I., Jaky, M. and Schelly, Z.A. (1984) Short-lived manganate(VI) and manganate(V) intermediates in the permanganate oxidation of sulfite ion. J Am Chem Soc 106, 6866-6867.

Stone, A.T. and Morgan, J.J. (1984) Reduction and dissolution of manganese(III) and manganese(IV) oxides by organics. 1. Reaction with hydroquinone. Environ. Sci. Technol. 18(6), 450-456.

Sun, B., Zhang, J., Du, J., Qiao, J. and Guan, X. (2013) Reinvestigation of the role of humic acid in the oxidation of phenols by permanganate. Environ. Sci. Technol. 47(24), 14332-14340.

Tian, S.H., Zhang, C., Huang, D.L., Wang, R.Z., Zeng, G.M., Yan, M., Xiong, W.P., Zhou, C.Y., Cheng, M., Xue, W.J., Yang, Y. and Wang, W.J. (2020) Recent progress in sustainable technologies for adsorptive and reactive removal of sulfonamides. Chem. Eng. J. 389.

Wang, W.J., Niu, Q.Y., Zeng, G.M., Zhang, C., Huang, D.L., Shao, B.B., Zhou, C.Y., Yang, Y., Liu, Y.X., Guo, H., Xiong, W.P., Lei, L., Liu, S.Y., Yi, H., Chen, S. and Tang, X. (2020) 1D porous tubular g-C3N4 capture black phosphorus

quantum dots as 1D/0D metal-free photocatalysts for oxytetracycline hydrochloride degradation and hexavalent chromium reduction. Appl. Catal., B-Environ. 273.

Webb, S.M., Dick, G.J., Bargar, J.R. and Tebo, B.M. (2005) Evidence for the presence of Mn(III) intermediates in the bacterial oxidation of Mn(II). Proc Natl Acad Sci USA 102(15), 5558-5563.

Xu, K., Ben, W., Ling, W., Zhang, Y., Qu, J. and Qiang, Z. (2017) Impact of humic acid on the degradation of levofloxacin by aqueous permanganate: Kinetics and mechanism. Water Res. 123, 67-74.

Xu, X., Chen, J., Wang, S., Ge, J., Qu, R., Feng, M., Sharma, V.K. and Wang, Z. (2018) Degradation kinetics and transformation products of chlorophene by aqueous permanganate. Water Res. 138, 293-300.

Xue, G., Zheng, M., Qian, Y., Li, Q., Gao, P., Liu, Z., Chen, H. and Li, X. (2020) Comparison of aniline removal by UV/CaO_2 and UV/H_2O_2: Degradation kinetics and mechanism. Chemosphere 255, 126983.

Yan, Y., E., Schwartz and F., W. (1999) Oxidative degradation and kinetics of chlorinated ethylenes by potassium permanganate. J Contam Hydrol 37(3–4), 343-365.

Yang, J.F., He, M., Wu, T.F., Hao, A.P., Zhang, S.B., Chen, Y.D., Zhou, S.B., Zhen, L.Y., Wang, R., Yuan, Z.L. and Deng, L. (2018) Sulfadiazine oxidation by permanganate: Kinetics, mechanistic investigation and toxicity evaluation. Chem. Eng. J. 349, 56-65.

Yang, W. and Parr, R.G. (1985) Hardness, softness, and the fukui function in the electronic theory of metals and catalysis. Proc Natl Acad Sci USA 82(20), 6723-6726.

Yang, Y., Li, X., Zhou, C., Xiong, W., Zeng, G., Huang, D., Zhang, C., Wang, W., Song, B., Tang, X., Li, X. and Guo, H. (2020) Recent advances in application of graphitic carbon nitride-based catalysts for degrading organic contaminants in water through advanced oxidation processes beyond photocatalysis: A critical review. Water Res. 184, 116200.

Yin, R.L., Guo, W.Q., Wang, H.Z., Du, J.S., Zhou, X.J., Wu, Q.L., Zheng, H.S., Chang, J.S. and Ren, N.Q. (2018) Enhanced peroxymonosulfate activation for sulfamethazine degradation by ultrasound irradiation: Performances and mechanisms. Chem. Eng. J. 335, 145-153.

Zhang, C., Lai, C., Zeng, G., Huang, D., Yang, C., Wang, Y., Zhou, Y. and Cheng, M. (2016a) Efficacy of carbonaceous nanocomposites for sorbing ionizable antibiotic sulfamethazine from aqueous solution. Water Res. 95, 103-112.

Zhang, C., Wang, W., Duan, A., Zeng, G., Huang, D., Lai, C., Tan, X., Cheng, M., Wang, R., Zhou, C., Xiong, W. and Yang, Y. (2019) Adsorption behavior of engineered carbons and carbon nanomaterials for metal endocrine disruptors: Experiments and theoretical calculation. Chemosphere 222, 184-194.

Zhang, R., Yang, Y., Huang, C.H., Zhao, L. and Sun, P. (2016b) Kinetics and modeling of sulfonamide antibiotic degradation in wastewater and human urine by UV/H_2O_2 and UV/PDS. Water Res. 103, 283-292.

Zhao, Y. and Truhlar, D.G. (2007) The M06 suite of density functionals for main group thermochemistry, thermochemical kinetics, noncovalent interactions, excited states, and transition elements: two new functionals and systematic testing of four M06-class functionals and 12 other functionals. Theor. Chem. Acc. 120(1-3), 215-241.

Zhao, Y. and Truhlar, D.G. (2008) Density functionals with broad applicability in chemistry. Acc Chem Res 41(2), 157-167.

Zhong, S. and Zhang, H. (2019) New insight into the reactivity of Mn(III) in bisulfite/permanganate for organic compounds oxidation: The catalytic role of bisulfite and oxygen. Water Res. 148, 198-207.

Zhou, C., Zeng, Z., Zeng, G., Huang, D., Xiao, R., Cheng, M., Zhang, C., Xiong, W., Lai, C., Yang, Y., Wang, W., Yi, H. and Li, B. (2019a) Visible-light-driven photocatalytic degradation of sulfamethazine by surface engineering of carbon nitrideProperties, degradation pathway and mechanisms. J. Hazard. Mater. 380, 120815.

Zhou, C.Y., Xu, P., Lai, C., Zhang, C., Zeng, G.M., Huang, D.L., Cheng, M., Hu, L., Xiong, W.P., Wen, X.F., Qin, L., Yuan, J.L. and Wang, W.J. (2019b) Rational design of graphic carbon nitride copolymers by molecular doping for visible-light-driven degradation of aqueous sulfamethazine and hydrogen evolution. Chem. Eng. J. 359, 186-196.

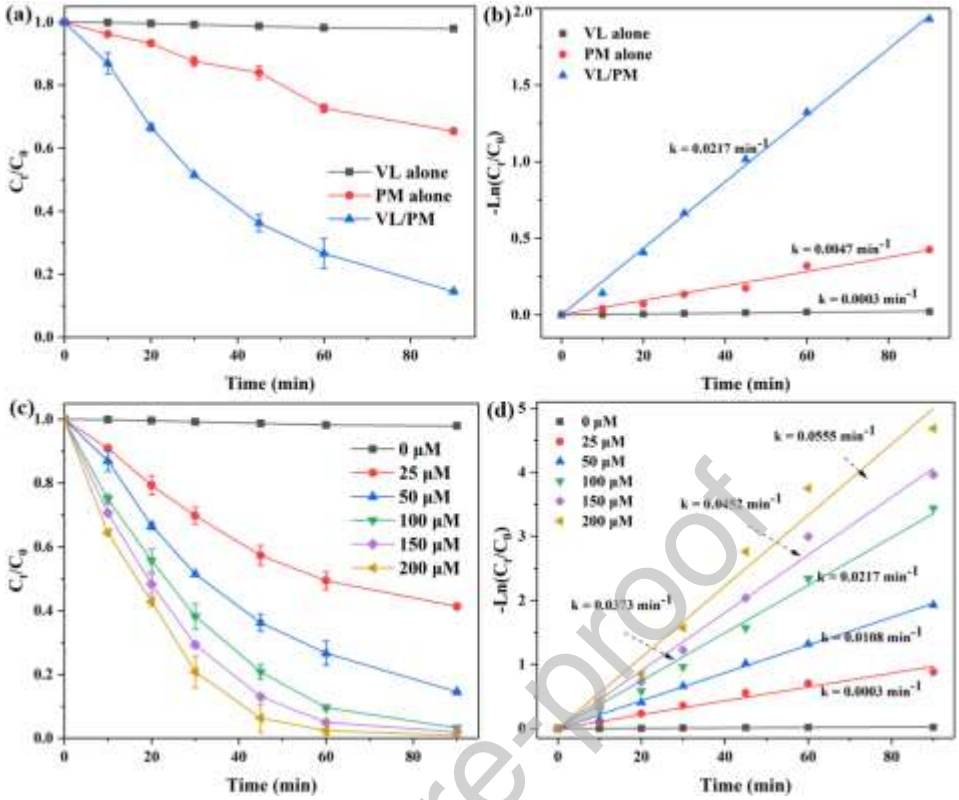

Figure 1. Degradation of SMT by VL alone, PM oxidation, VL/PM process. (a) Degradation efficiency and (b) the corresponding degradation rate constants. (c) Effect of PM dosage on SMT degradation by VL/PM process and (d) the corresponding degradation rate constants. Reaction conditions: $[PM]_0$ = 50 μM, $[SMT]_0$ = 10 mg/L, original pH= 6.43, and T = 25 °C.

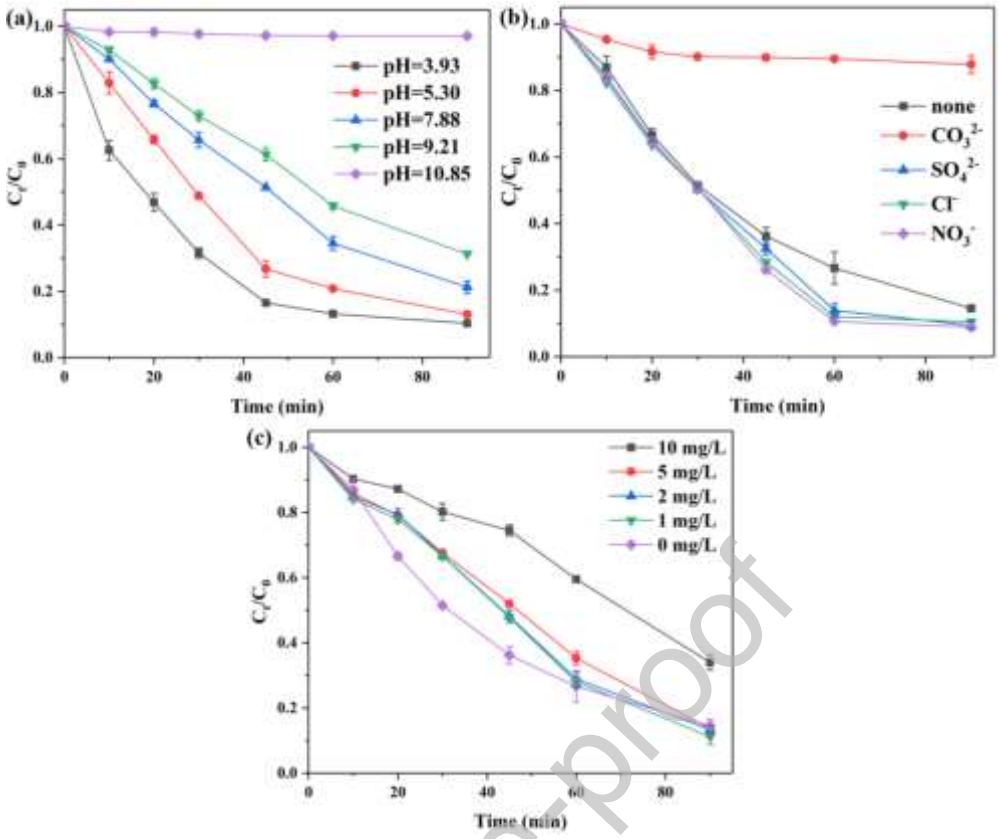

Figure 2. Effect of (a) solution pH, (b) anions ($[CO_3^{2-}] = [SO_4^{2-}] = [Cl^{-1}] = [NO_3^-] =$ 0.5 mM) and (c) HA on VL/PM mediated degradation of SMT. Reaction conditions: $[PM]_0$ = 50 μM, $[SMT]_0$ = 10 mg/L, [HA] = 0-10 mg/L, original pH= 6.43, and T = 25 °C.

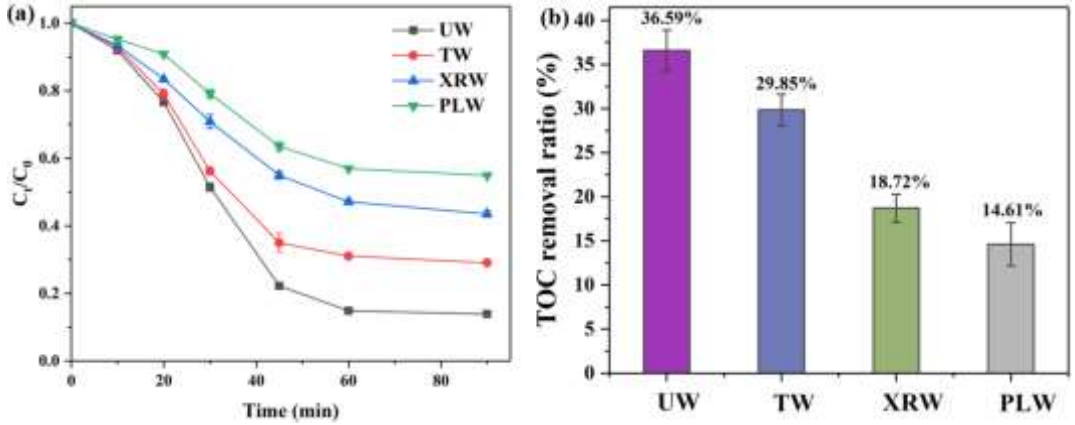

Figure 3. Oxidation performance of (a) PM and (b) TOC removal rate in different real water. Reaction conditions: $[PM]_0$ = 50 μM, $[SMT]_0$ = 10 mg/L, pH= 7.88, and T = 25 °C.

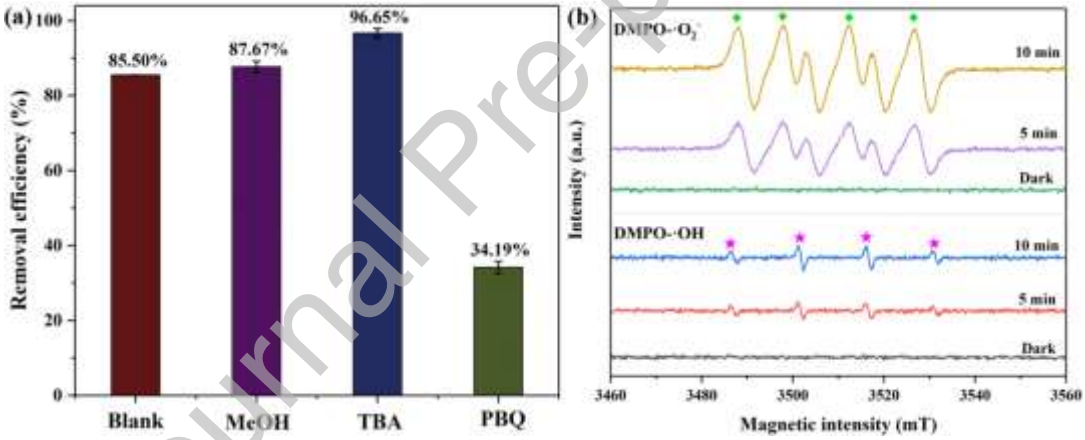

Figure 4. (a) Quenching results of different free radical scavengers. Reaction conditions: reaction time = 90 min, $[PM]_0$ = 50 μM, $[SMT]_0$ = 10 mg/L, [MeOH] = [TBA] = 40 mM, [PBQ] = 2 mM, original pH= 6.43, and T = 25 °C. (b) ESR spectra of DMPO-•O_2^- and DMPO-•OH in VL/PM system.

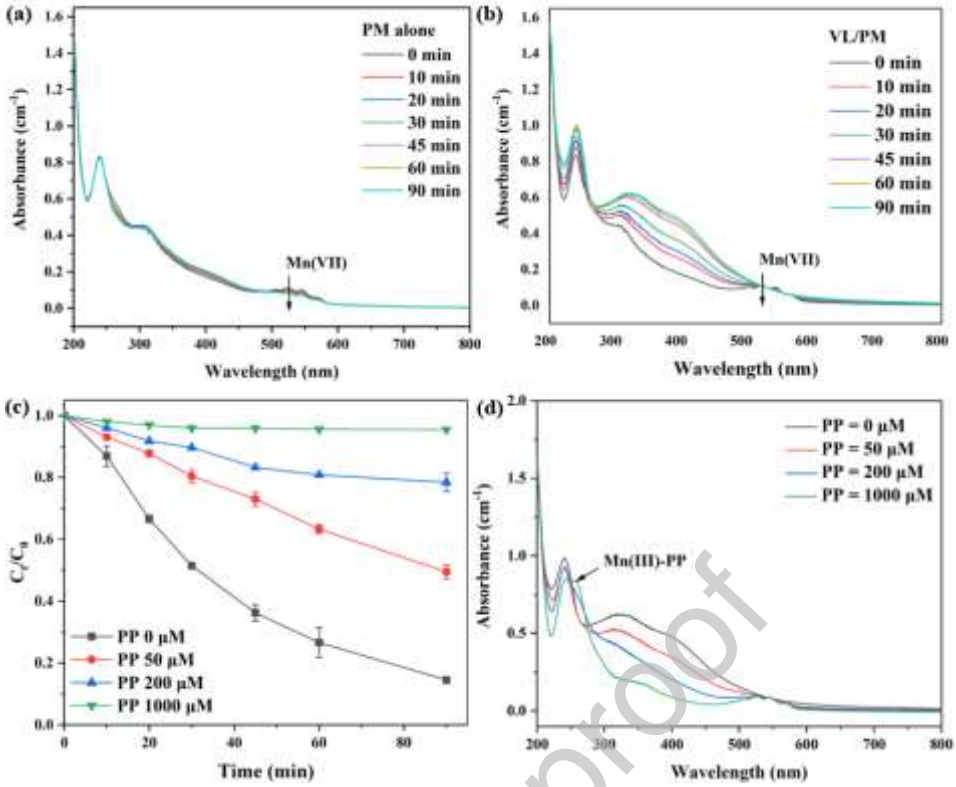

Figure 5. The evolution of UV-vis spectra at 200 nm-800 nm containing PM+ SMT (a) in the PM oxidation system and (b) VL/PM system. (c) The effect of PP on the degradation of SMT in VL/PM system and (d) corresponding UV-vis spectra after 90 min reaction. Reaction conditions: $[PM]_0$= 50 μM, $[SMT)]_0$=10 mg/L, pH= 6.43.

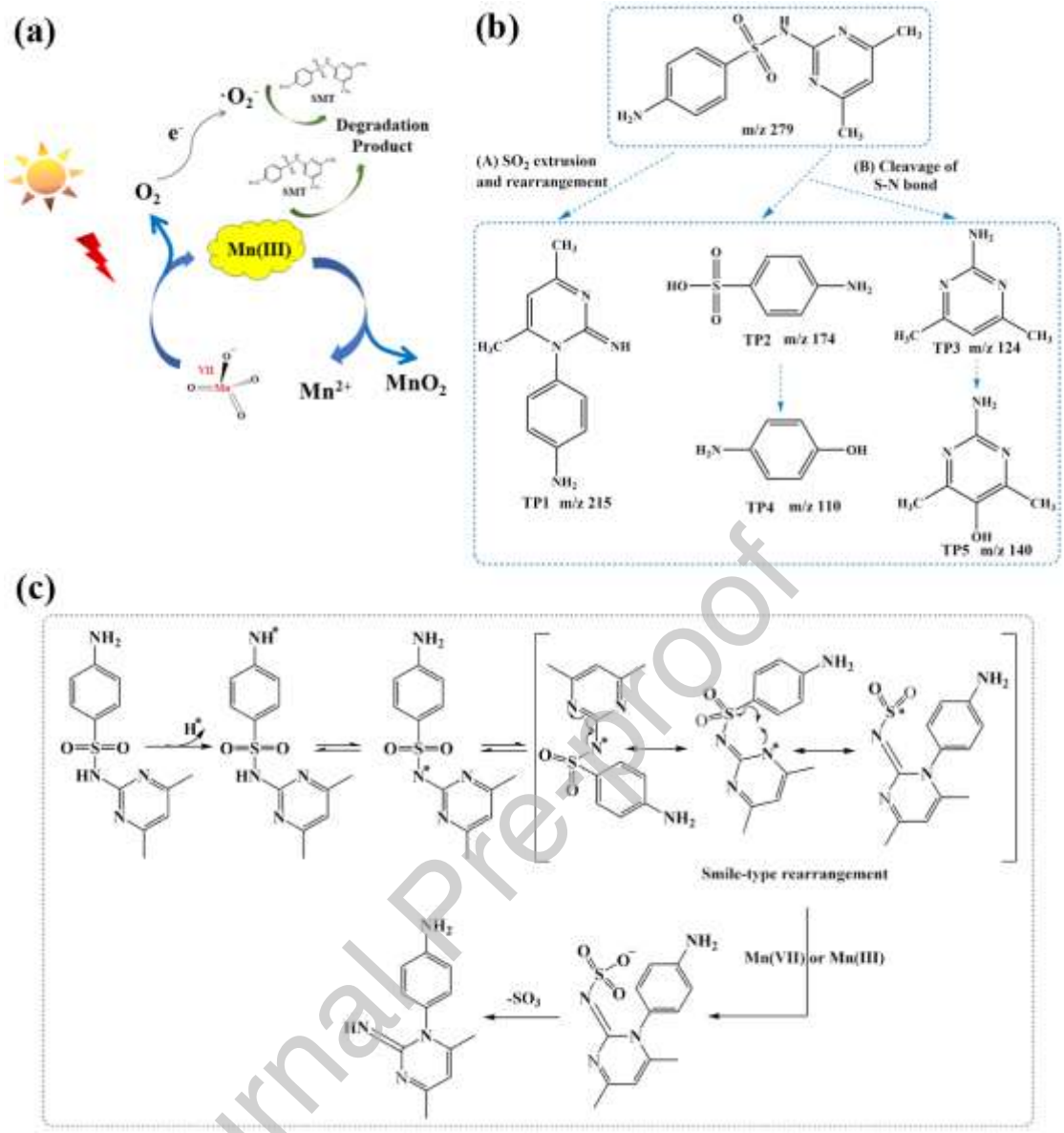

Figure 6. (a) Proposed mechanism for the reactive species under the VL/PM system. (b) Possible degradation pathway of SMT by VL/PM; (c) Schematic diagram of pathway A: smiles-type rearrangement and SO_2 extrusion.

(a)

(b)

Atom	Site	q(N)	q(N+1)	q(N-1)	f⁺	f⁻	f⁰	CDD
C	1	-0.0609	-0.0897	-0.0176	0.0433	0.0288	0.0360	-0.0145
C	2	-0.0232	-0.0655	0.0003	0.0234	0.0423	0.0329	0.0189
C	3	-0.0505	-0.0870	-0.0073	0.0433	0.0365	0.0399	-0.0068
C	4	-0.0271	-0.0613	-0.0046	0.0225	0.0342	0.0284	0.0117
C	5	-0.0625	-0.0944	-0.0127	0.0497	0.0320	0.0409	-0.0177
C	6	0.0616	0.0024	0.0980	0.0365	0.0591	0.0478	0.0227
C	11	0.0837	0.0171	0.1104	0.0267	0.0666	0.0466	0.0399
C	12	-0.0783	-0.1089	-0.0120	0.0663	0.0306	0.0485	-0.0357
C	13	0.0771	0.0165	0.1043	0.0272	0.0606	0.0439	0.0334
C	14	0.1502	0.1295	0.1684	0.0182	0.0206	0.0194	0.0025
N	16	-0.1938	-0.2536	-0.1594	0.0344	0.0598	0.0471	0.0253
N	17	-0.1710	-0.2142	-0.1431	0.0278	0.0432	0.0355	0.0154
C	18	-0.0814	-0.1009	-0.0705	0.0109	0.0195	0.0152	0.0086
C	22	-0.0792	-0.0989	-0.0681	0.0110	0.0198	0.0154	0.0087
N	26	-0.1343	-0.1456	-0.0779	0.0565	0.0113	0.0339	-0.0452
S	28	0.5093	0.4819	0.5315	0.0223	0.0274	0.0248	0.0051
O	29	-0.3255	-0.3578	-0.2787	0.0468	0.0323	0.0396	-0.0145
O	30	-0.3306	-0.3616	-0.2701	0.0605	0.0309	0.0457	-0.0296
N	31	-0.1587	-0.1983	-0.0679	0.0908	0.0396	0.0652	-0.0512

(c)

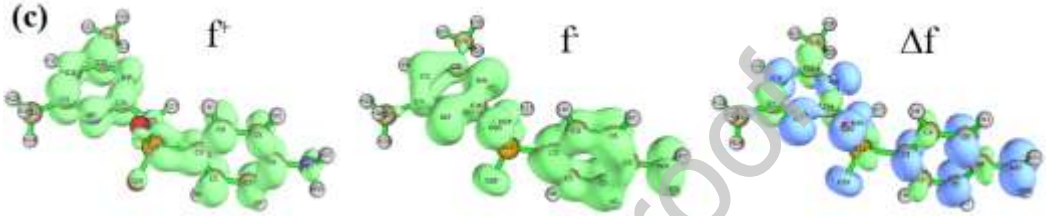

Figure 7. (a) SMT chemical structure (gray, carbon; white, hydrogen; red, oxygen; blue, nitrogen; yellow, sulfur), (b) Condensed Fukui index distribution on SMT, (c) the isosurface of Fukui index (The blue and green colors represent the negative and positive phases of the molecular orbital).

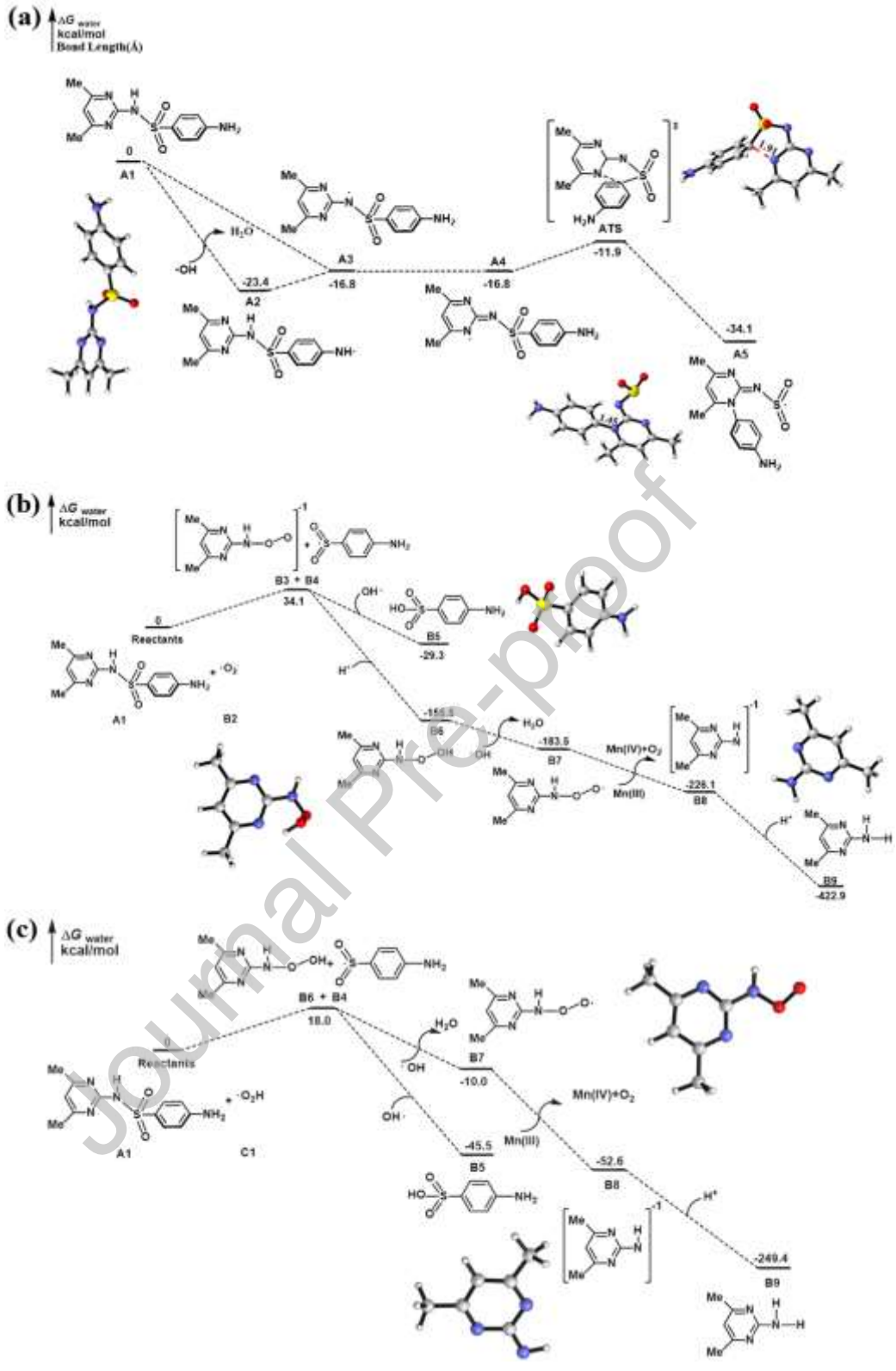

Figure 8. The computed potential energy profile for SMT degradation pathways (a) smiles-type rearrangement and SO_2 extrusion, (b) cleavage of S–N bond of SMT by reaction with $\bullet O_2^-$ and (c) cleavage of S–N bond of SMT by reaction with $\bullet O_2H$.

Graphical Abstract